

A Comparison of Void-Finding Algorithms using Crossing Numbers

DAHLIA VEYRAT,¹ KELLY A. DOUGLASS,¹ AND SEGEV BENZVI¹

¹*Department of Physics & Astronomy, University of Rochester, 500 Wilson Blvd., Rochester, NY 14627*

ABSTRACT

We study how well void-finding algorithms identify cosmic void regions and whether we can quantitatively and qualitatively compare the voids they find with dynamical information from the underlying matter distribution. Using the ORIGAMI algorithm to determine the number of dimensions along which dark matter particles have undergone shell-crossing (crossing number) in N -body simulations from the AbacusSummit simulation suite, we identify dark matter particles that have undergone no shell crossing as belonging to voids. We then find voids in the corresponding halo distribution using two different void-finding algorithms: VoidFinder and V^2 , a ZOBOV-based algorithm. The resulting void catalogs are compared to the distribution of dark matter particles to examine how their crossing numbers depend on void proximity. While both algorithms' voids have a similar distribution of crossing numbers near their centers, we find that beyond 0.25 times the effective void radius, voids found by VoidFinder exhibit a stronger preference for particles with low crossing numbers than those found by V^2 . We examine two possible methods of mitigating this difference in efficacy between the algorithms. While we are able to partially mitigate the ineffectiveness of V^2 by using the distance from the void edge as a measure of centrality, we conclude that VoidFinder more reliably identifies dynamically distinct regions of low crossing number.

1. INTRODUCTION

On cosmic scales, the structure of matter in the observable universe exhibits a complex, web-like distribution (Bond et al. 1996), with distinct filaments stretching between dense clusters of galaxies. In the space between these superstructures, galaxy redshift surveys have found vast, relatively empty regions containing very few galaxies (Jöeveer et al. 1978; Gregory & Thompson 1978; Kirshner et al. 1981). These cosmic voids, which occupy most of the volume of the universe (de Lapparent et al. 1986; Geller & Huchra 1989), are the result of the gravitational instability in primordial underdense regions, similar to the formation of clusters from gravitational collapse of primordial overdensities (Zeldovich 1970; van de Weygaert & Platen 2011).

The emptiness of voids provides a unique environment of gravitational evolution for cosmological and astrophysical studies. Cosmologically, the lack of large-scale gravitational collapse causes dynamics within voids to remain in the linear regime for a relatively longer time (Goldberg & Vogeley 2004). Their uniqueness as cosmic structures has made voids well-suited to studies of the Alcock-Paczyński effect (e.g. Lavaux & Wandelt 2012; Sutter et al. 2012, 2014; Hamaus et al. 2016; Mao et al. 2017; Nadathur et al. 2019), dark energy (e.g. Pisani et al. 2015; Verza et al. 2019), baryon acoustic oscillations (e.g. Nadathur et al. 2019; Zhao et al. 2020, 2022), and weak lensing (e.g. Melchior et al. 2014; Chantavat et al. 2017). Additionally, the uniqueness of voids as an intergalactic environment results in measurably different evolution and properties of galaxies within them (e.g. Hoyle et al. 2005; Rojas et al. 2005; Patiri et al. 2006; Douglass et al. 2019; Habouzit et al. 2020).

A number of different types of algorithms have been used to detect voids in the cosmic web. The VoidFinder algorithm (El-Ad & Piran 1997; Hoyle & Vogeley 2002) finds relatively empty spheres in the distribution of galaxies and combines them into individual voids. Another common strategy is to link low-density regions to-

Corresponding author: Dahlia Veyrat
dveyrat@ur.rochester.edu
kellyadouglass@rochester.edu
segev.benzvi@rochester.edu

gether using a watershed algorithm. Several implementations using a Voronoi tessellation to approximate local density exist (e.g. Neyrinck 2008; Sutter et al. 2015; Nadathur et al. 2019).

While the aforementioned algorithms find voids geometrically, voids are expected to be dynamically unique structures (Sheth & van de Weygaert 2004). This dynamical information is not typically available in galaxy redshift surveys, but with simulations, it is possible to define voids relative to the dynamics of the matter within them. Cosmological simulations have been used to predict properties of voids (Ricciardelli et al. 2014; Hamaus et al. 2014) and forecast the cosmological constraining power of voids (Pisani et al. 2015). One method for identifying dynamical voids in simulations is the computation of the number of dimensions along which matter has gravitationally collapsed (Falck et al. 2012). As described in Section 4, voids are defined as regions undergoing no shell-crossing.

In this work, we investigate the ability of geometrical void-finding algorithms to detect dynamical void regions. We apply the ORIGAMI algorithm (Falck et al. 2012) to an N -body simulation from the AbacusSummit simulation suite (Maksimova et al. 2021) to determine each dark matter particle’s crossing number — the number of dimensions along which it undergoes shell-crossing (the number of dimensions of gravitational collapse). Then, using the crossing numbers to classify particles as belonging to voids, walls, filaments, or clusters, we study the overlap of these categories with the voids found in the corresponding halo catalog identified by two different void-finding algorithms in the Void Analysis Software Toolkit (VAST; Douglass et al. 2022): VoidFinder and V^2 . This allows us to quantify the relative accuracy of these algorithms in detecting dynamically distinct regions, i.e. regions dominated by low crossing numbers, of the large scale structure.

The paper is organized as follows. In Section 2, we describe the theory of void evolution relevant to our study, and in Section 3, we describe the AbacusSummit simulation suite and the properties of the simulation used in the crossing number analysis. Sections 4 and 5 present the algorithms used to compute crossing numbers of dark matter particles and to find voids in the distribution of halos, respectively. Results are discussed in Section 6, examining the relationships between void regions defined by void-finding algorithms and the void particles identified by ORIGAMI. In Section 7, we explore ways to mitigate the relatively poor classification of the watershed algorithm, V^2 , and in Section 8, we summarize our results.

2. EXCURSION FORMALISM

The excursion-set formalism, first proposed by Press & Schechter (1974), provides an analytical model of the gravitational collapse and virialization of dark matter halos. Bond et al. (1991) developed the excursion model to describe the halo mass function, but the model was not applied to a theoretical description of voids until the pioneering work of Sheth & van de Weygaert (2004).

The excursion-set model of voids describes the evolution of an initial underdensity in the matter distribution. Sheth & van de Weygaert (2004) find that, as matter is attracted to the overdense surroundings, the typical shape of underdensities becomes more spherical and can be effectively described by a series of spherical shells. More central shells experience a stronger “repulsion” from void centers, leading to a distinct “wall” feature — a build up of expanding matter near the void edge as shells approach and cross each other. We expect, then, to find a high but narrow preference for high dark matter particle crossing numbers (the number of dimensions along which they have undergone shell-crossing) near void edges, along with the preference for low crossing numbers in voids’ more central regions.

It is also possible to use the excursion-set formalism to model the theoretical abundance of spherical underdensities in the Universe. While we expect good agreement between low crossing numbers and void regions due to the dynamical processes involved in void formation, crossing numbers are not useful for identifying the distinct spherical underdensities whose abundance is described by Sheth & van de Weygaert (2004).

3. SIMULATIONS

The AbacusSummit simulation suite (Maksimova et al. 2021) is a set of over 100 periodic N -body simulations spanning several box sizes up to $(7.5 \text{ Gpc}/h)^3$, particle mass resolutions down to $\sim 3 \times 10^8 M_\odot$, and implementing several cosmologies. AbacusSummit was produced with the Abacus N -body algorithm (Garrison et al. 2021) at the Oak Ridge Leadership Computing Facility’s Summit supercomputer and is the largest high-accuracy N -body data set produced to date.

We use an AbacusSummit Hugebase simulation, which evolves 2304^3 dark matter particles of mass $\sim 5 \times 10^{10} M_\odot$ within a periodic box of side length $2 \text{ Gpc}/h$. This simulation uses Planck 2018 flat Λ CDM cosmology: $\Omega_m = 0.315$, $h = 0.674$, $\sigma_8 = 0.811$, $n_s = 0.965$ (Planck Collaboration et al. 2020). In addition to full particle timeslices, the AbacusSummit data products include halo catalogs produced using the CompaSO halo-finder (Hadzhiyska et al. 2021). We run all void-finding algo-

rithms on the corresponding halo catalog of the Hugebase simulation, which contains $\sim 1.8 \times 10^7$ halos.

4. CROSSING NUMBERS USING ORIGAMI

The gravitational collapse of the matter distribution in these N -body simulations results in the crossing of dark matter particle positions as their dynamics become nonlinear. The number of dimensions of shell-crossing, and thus of nonlinearity, determines the classification of dark matter particles into various types of large-scale structures: clusters from three-dimensional collapse, filaments from two-dimensional collapse, and walls from one-dimensional collapse. Particles which have undergone no shell-crossing are defined as belonging to cosmic voids. The ORIGAMI algorithm (Falck et al. 2012) computes the number of shell-crossing dimensions, referred to as the crossing number (CN), by comparing the final relative positions of pairs of particles with their relative positions on the initial grid.

Running the base ORIGAMI algorithm on simulations with more than 512^3 particles requires a prohibitively large amount of memory. We introduce modifications that compute crossing numbers for subvolumes of periodic simulations by implementing a buffer zone and subsequently merge the subvolume results, allowing ORIGAMI to be run on larger simulations. Crossing numbers in the AbacusSummit simulations were computed using this modified version of ORIGAMI¹.

5. VAST

We identify voids in the distribution of halos using the Void Analysis Software Toolkit² (VAST; Douglass et al. 2022). VAST includes an implementation of the VoidFinder algorithm, which grows and merges nearly empty spheres, and V^2 , an implementation of the ZOBOV algorithm (Neyrinck 2008), which uses a watershed method to identify voids. The voids found by each algorithm are shown in Figure 1, overlaying the dark matter particles within a $10 \text{ Mpc}/h$ -thick slice of the AbacusSummit Hugebase simulation.

5.1. *VoidFinder*

VoidFinder, originally described by El-Ad & Piran (1997), begins by removing isolated tracers from the catalog, defined as those with a distance to their third-nearest neighbor $d_{3\text{NN}} > \overline{d_{3\text{NN}}} + 1.5\sigma_{d_{3\text{NN}}}$. The remaining tracers are placed on a three-dimensional grid, and

a sphere is grown from each empty grid cell until its surface is bounded by four tracers. Next, maximal spheres, defined as spheres with radii $r \geq 10 \text{ Mpc}/h$ that do not overlap a larger maximal sphere by more than 10% of their volume, are selected from the population of spheres. Each maximal sphere is identified as belonging to a unique void, and that void is built from the union of all spheres which intersect exactly one maximal sphere by at least 50% of their volume. See Hoyle & Vogeley (2002) for a more detailed description of VoidFinder.

5.2. *Voronoi Voids (V^2)*

Voronoi Voids, or V^2 , is a Python implementation of the ZOBOV algorithm, first described in Neyrinck (2008). V^2 begins by creating a Voronoi tessellation of the tracer distribution, whose cell volumes are used as estimates of the local density. A watershed algorithm is used to combine groups of adjacent Voronoi cells into “zones,” where each cell is put into the same zone as its least dense neighboring cell, and any cell which is less dense than any of its neighbors is identified as a local density minimum that serves as its zone’s central cell.

Adjacent zones are linked together by the least-dense pair of adjacent cells between them, whose density is referred to as the “linking density.” The collections of linked zones (including single zones) are identified as voids, creating a hierarchy of voids up to one containing the entire catalog. Several methods exist to prune the full hierarchy and extract meaningful voids (see Neyrinck 2008; Sutter et al. 2015; Nadathur et al. 2019). We use two pruning methods: VIDE pruning (V^2 /VIDE, Sutter et al. 2015), which sets a maximum linking density for the zone-linking step, an optional maximum central density for each void, and a minimum void radius (we use $10 \text{ Mpc}/h$ in this work); and REVOLVER pruning (V^2 /REVOLVER, Nadathur et al. 2019), which labels each zone as a unique void. To our implementation of REVOLVER we add the option to remove any voids with effective radii less than the median void effective radius.

There are several methods for computing the centers of ZOBOV voids. For most of the pruning methods, the default void center definition in V^2 is the barycenter of the tracers within the void, weighted by the volumes of their Voronoi cells. The default for the V^2 /REVOLVER pruning algorithm is the center of the largest empty sphere which can be inscribed in the void. In our tests of V^2 /REVOLVER, we use both of these definitions of void centers.

6. RESULTS

¹ The modified ORIGAMI is available for download at <https://github.com/dveyrat/origami/tree/subdivide>.

² VAST is available for download at <https://github.com/desi-ur/vast>.

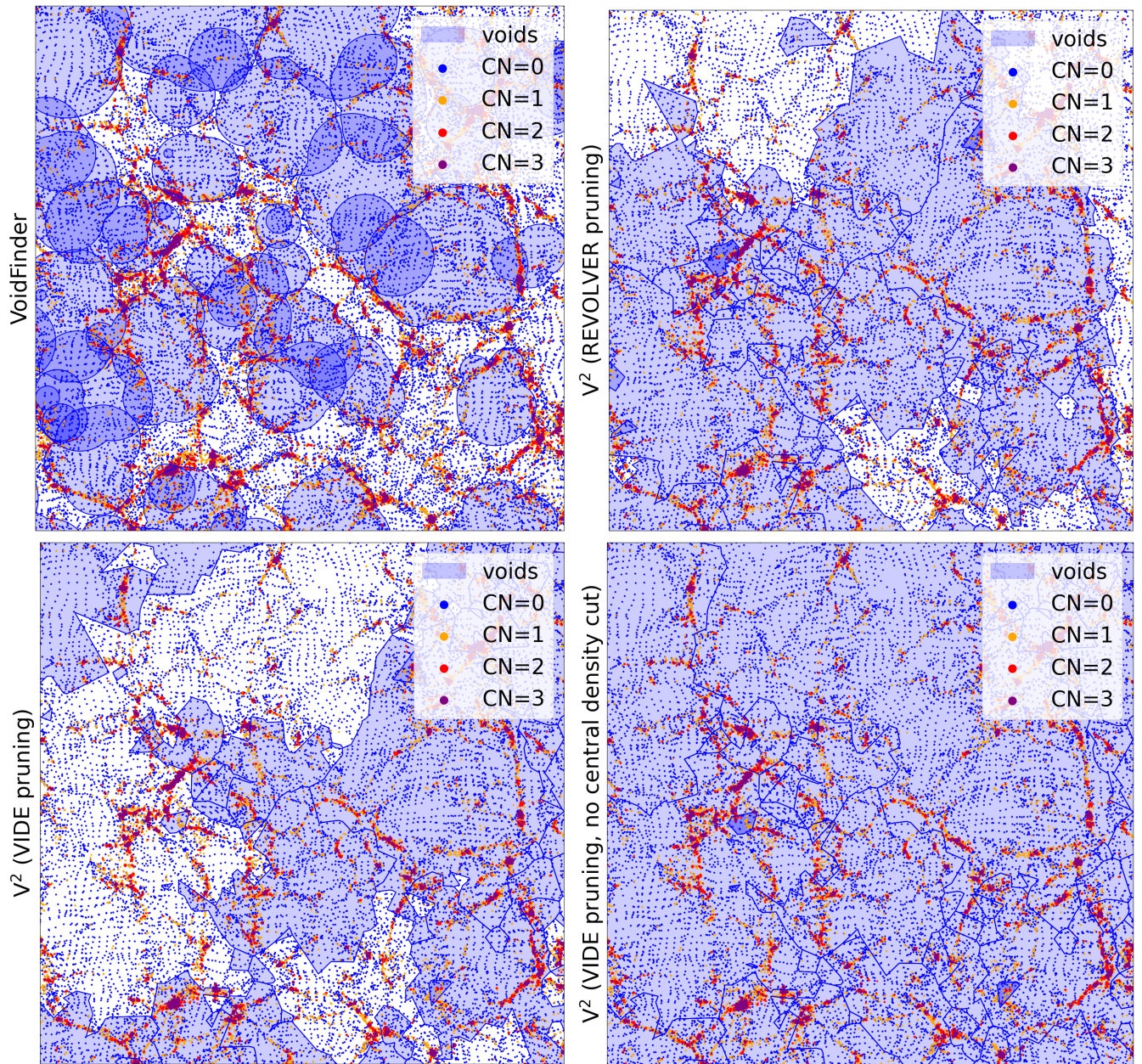


Figure 1. A $100 \text{ Mpc}/h \times 100 \text{ Mpc}/h$ subsection of a $10 \text{ Mpc}/h$ -thick slice of the AbacusSummit Hugebase simulation. The locations of particles with crossing number 0 are shown in blue, 1 in orange, 2 in red, and 3 in violet. The intersections of voids with the center of the slice are shown in blue for VoidFinder (top left), V^2 /REVOLVER (top right), and V^2 /VIDE (bottom).

A total of 410,852 voids were found in the Abacus Hugebase simulation by VoidFinder, 79,721 voids by V^2 /VIDE, 81,680 voids by V^2 /VIDE with no central density cut³, and 43,430 voids by V^2 /REVOLVER. The fraction of dark matter particles with each crossing number in the AbacusSummit Hugebase simulation, and of

those in voids defined by each of the void-finding algorithms studied, can be found in Table 1. Throughout the entire simulation, we find that 31% of the dark matter particles have undergone no shell-crossing, 19% have undergone shell-crossing along one dimension, 18% along two dimensions, and 32% along three dimensions. These results are in good agreement with the crossing number distributions found by Falck & Neyrinck (2015) for similar particle resolutions. Our results, using a simulation with an initial grid spacing $L/N = (1000 \text{ Mpc}/h)/1152$, are similar to those in Falck & Neyrinck (2015) for initial

³ 872 voids with $R_{\text{eff}} > 80 \text{ Mpc}/h$ were removed from this catalog to prevent the inclusion of large supervoids in the void hierarchy containing most of the survey.

Table 1. Crossing number distributions

Crossing Number:	0	1	2	3
all DM particles	30.8%	19.4%	18.2%	31.6%
particles in VoidFinder voids	46.9%	22.4%	15.6%	15.0%
particles not in VoidFinder voids	16.6%	16.6%	20.5%	46.3%
particles in V ² /VIDE voids	30.6%	19.4%	18.2%	31.8%
particles not in V ² /VIDE voids	31.3%	19.4%	18.1%	31.2%
particles in V ² /VIDE voids, no central density cut	30.6%	19.3%	18.2%	31.9%
particles not in V ² /VIDE voids, no central density cut	34.4%	19.9%	17.7%	28.1%
particles in V ² /REVOLVER voids	31.3%	19.4%	18.1%	31.2%
particles not in V ² /REVOLVER voids	28.7%	19.1%	18.5%	33.6%

NOTE—Distribution of crossing numbers inside and outside of voids found by VoidFinder and V², as well as the total distribution in the AbacusSummit Hugebase simulation. We report the fraction of particles in a region with a given crossing number. For example, 46.9% of all particles in VoidFinder voids have CN = 0. All uncertainties are below 0.1%, estimated using several AbacusSummit Hugebase realizations.

Table 2. CN = 0 particles not in voids

VoidFinder	V ² /VIDE	V ² /VIDE, <i>nocentral densitycut</i>	V ² /REVOLVER
28.4%	36.4%	8.3%	14.6%

NOTE—Percentage of particles with CN = 0 particles not located in any void found by VoidFinder and V². All uncertainties are below 0.1%, estimated using several AbacusSummit Hugebase realizations.

grid spacing $L/N = (100 \text{ Mpc}/h)/128$ but with a shift towards more void (CN = 0) particles and fewer cluster (CN = 3) particles, agreeing with the trend for greater initial grid spacing.

6.1. Crossing Number Distribution within Voids

We expect the distribution of crossing numbers in void regions to contain an excess of CN = 0 particles because any dark matter particles which are identified by ORIGAMI to have undergone shell-crossing are expected to be part of a gravitationally bound structure: either wall, filament, or cluster. To determine the effectiveness of VoidFinder and V² at detecting regions with low crossing number, we examine the distribution of crossing numbers inside and outside voids. We observe that the distributions of dark matter particles with CN = 0 (void particles) and CN = 3 (cluster particles) differ significantly when the particles are catego-

rized by whether they are inside or outside a void (Table 1). The distributions of CN = 1 and CN = 2 particles differ relatively little between void/non-void regions. While particles in voids are more likely to have CN = 0 and less likely to have CN = 3 than the background distribution, this preference is significantly stronger in VoidFinder voids, where 47% of particles within the voids have CN = 0 compared to 31% in V²/VIDE and V²/REVOLVER voids, and 31% overall; only 15% of particles in VoidFinder voids have CN = 3, compared to 32% in V²/VIDE voids, 34% in V²/VIDE voids with no central density cut, 31% in V²/REVOLVER voids, and 32% overall.

Figure 2 shows the crossing number density profiles of dark matter particles around voids, and Figure 3 shows how the distribution of crossing numbers is related to the normalized distance to void centers, r/R_{eff} , where the effective radius R_{eff} is defined as the radius of a sphere with the same volume as the void. We find that the particles closest to void centers are significantly more likely to have crossing number 0 than 3 for both VoidFinder and V². However, while this preference for low crossing numbers extends to nearly $r = R_{\text{eff}}$ for VoidFinder voids, the distribution around V² voids begins to gradually shift toward the background crossing number distribution at $r \approx 0.25R_{\text{eff}}$ for V²/VIDE voids, and $r \approx 0$ for V²/REVOLVER voids and V²/VIDE voids with no central density cut. At a normalized distance of $r \approx 0.8R_{\text{eff}}$, the distribution of crossing numbers in V² voids is nearly identical to the background.

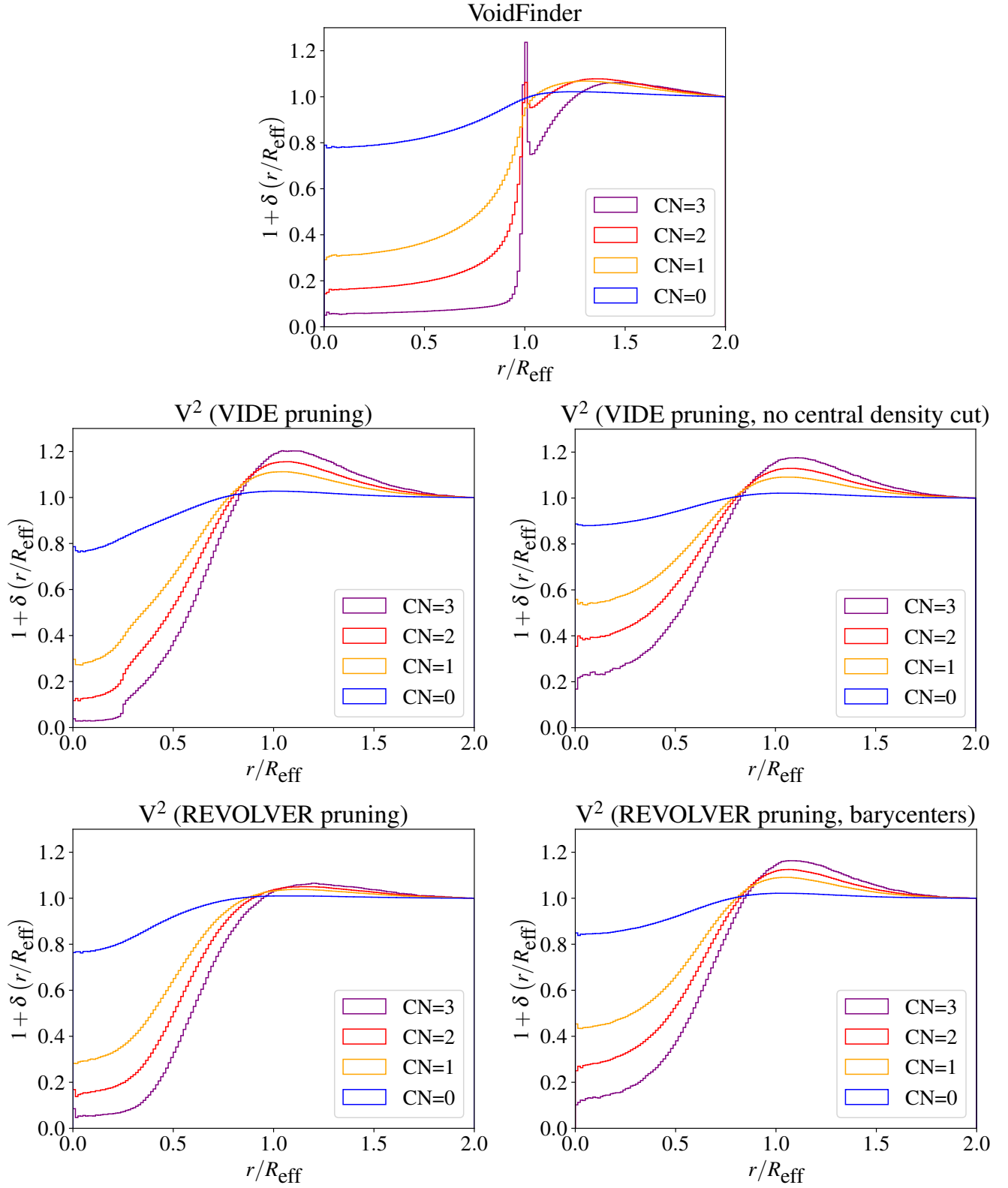


Figure 2. Normalized void density profiles by crossing number for VoidFinder (top), V²/VIDE (middle), and V²/REVOLVER (bottom) voids. All uncertainties are negligibly small, estimated using several AbacusSummit Hugebase realizations.

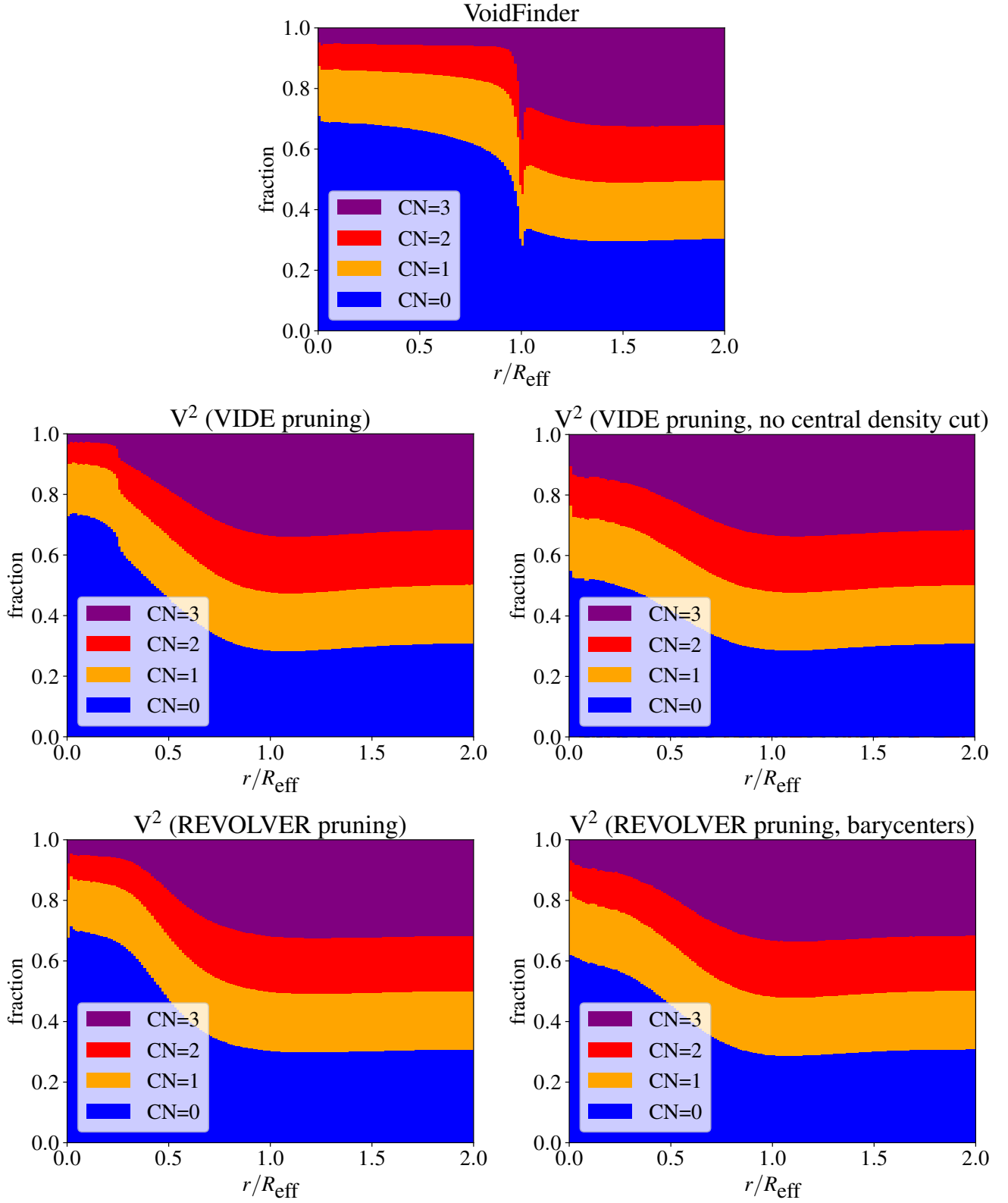


Figure 3. The distributions of crossing numbers by normalized distance from void centers found in real space by VoidFinder (top), V²/VIDE (middle), and V²/REVOLVER (bottom).

The expected wall feature of voids is visually evident in both Figures 2 and 3, but it is more prominent around voids found by VoidFinder. There is a clear, sharp increase in preference for higher crossing numbers near $r = R_{\text{eff}}$, in good agreement with the theory developed in Sheth & van de Weygaert (2004), which predicts a build-up and crossing of mass shells as they expand radially outward from void centers (see Section 2 for details). The wall feature around V^2 voids is both less pronounced and less localized around $r = R_{\text{eff}}$.

We also observe a sharp feature at $r = 0.25R_{\text{eff}}$ in the distributions of crossing numbers in V^2/VIDE voids when the central density cut is applied. This is an artifact of the central density cut, which removes all voids with densities above some threshold within $r < 0.25R_{\text{eff}}$. As seen in the middle right panel of Figures 2 and 3, the distribution of crossing numbers around voids found by V^2/VIDE with no central density cut lacks this feature.

6.2. $CN=0$ Particles not in Voids

While the majority of particles with crossing number 0 are located within VoidFinder voids, 28% do not fall within a void. And, while particles with lower crossing numbers are more likely to be found within V^2 voids than those with higher crossing numbers, 36% of $CN=0$ particles do not fall within a V^2/VIDE void, 8% do not fall within a V^2/VIDE void with no central density cut, and 15% do not fall within a $V^2/\text{REVOLVER}$ void.

To determine whether these particles belong to regions we expect to be classified as void, we investigate their local environments. For each dark matter particle, we identify all particles within 2 Mpc/ h and count the particles with a given crossing number. In a void-like environment, we expect fewer neighboring particles with higher crossing numbers, as well as a lower density of particles overall, leading to a lower particle count for $CN > 0$ particles relative to $CN=0$ and a lower total particle count.

The crossing numbers within 2 Mpc/ h of $CN=0$ particles inside and outside of voids are shown in Table 3 for both VoidFinder and V^2 . Overall, $CN=0$ particles are found to be located in void-like environments with little clustering ($CN > 0$ particles). $CN=0$ particles outside of VoidFinder voids, however, tend to be located in environments with more neighboring particles overall and several times more $CN > 0$ particles than in the local environments of $CN=0$ particles in VoidFinder voids. This suggests that, while dynamical information alone classifies all $CN=0$ particles as belonging to void regions, many are located in significantly denser environments and subsequently do not belong to cosmic

Table 3. Local environment of $CN=0$ particles

Crossing Number:	0	1–3	total
all	19 (11, 28)	11 (0, 61)	32 (13, 86)
VoidFinder:			
– inside voids	18 (11, 27)	7 (0, 41)	28 (12, 67)
– outside voids	21 (13, 30)	27 (3, 121)	51 (20, 146)
V^2/VIDE :			
– inside voids	19 (11, 28)	11 (0, 61)	33 (14, 87)
– outside voids	19 (11, 28)	10 (0, 59)	32 (13, 85)
V^2/VIDE , no central density cut:			
– inside voids	19 (11, 28)	11 (0, 62)	33 (14, 87)
– outside voids	18 (10, 27)	9 (0, 52)	29 (12, 77)
$V^2/\text{REVOLVER}$:			
– inside voids	19 (11, 28)	10 (0, 60)	32 (13, 86)
– outside voids	19 (11, 28)	12 (0, 65)	34 (14, 90)

NOTE—Median number of particles < 2 Mpc/ h from particles with $CN=0$ that fall inside or outside a void. Values in parentheses indicate the boundaries of the central 68% of the distribution.

voids. These are therefore expected to not be located in VoidFinder voids.

The local environments of $CN=0$ particles in V^2 voids, however, are much more similar to those of their undetected counterparts and of $CN=0$ particles as a whole. Like the overall crossing number distributions in Table 1, this indicates worse classification of void regions by V^2 , with no evident environmental distinction between the $CN=0$ particles inside voids and those outside.

6.3. Void Finding in Redshift Space

We also run both void-finding algorithms on a version of the halo catalog modified using peculiar velocity information to simulate the effect of peculiar velocities on apparent positions, an effect known as redshift-space distortions (RSDs). Because peculiar velocities within voids tend to be directed outwards, voids appear elongated along the line-of-sight in redshift space, and we expect a smoothing of features in the radial distribution of crossing numbers around voids.

Figure 4 shows how the distribution of crossing numbers is related to normalized distance to void centers found in redshift space. While the distributions are similar to those shown in Figure 3 at low and high r/R_{eff} , the distinct features at $r/R_{\text{eff}} = 1$ for VoidFinder and $r/R_{\text{eff}} = 0.25$ for V^2/VIDE appear to be smoothed out, as expected due to the distortion of the voids along the line of sight. This suggests that performing reconstruc-

tion of real-space positions in a redshift catalog before running a void-finding algorithm may improve the voids found.

6.4. Summary of Results

We expect void regions to contain an excess of particles with CN= 0 relative to the background distribution, and voids found by both VoidFinder and V^2 contain such an excess. In V^2 voids, however, there is a strong excess only in the most central ($r < 0.25R_{\text{eff}}$) regions, while in VoidFinder voids it extends nearly to R_{eff} . Further, there is an excess of CN= 3 (cluster) particles near the edge of VoidFinder voids, in agreement with dynamical theories of void evolution. We conclude that VoidFinder identifies void regions more accurately than V^2 . While this is particularly relevant for studies of astrophysics in the void environment, it is less indicative of performance in cosmological void analyses, which depend more on the identification of void centers than void regions.

7. MITIGATING POOR CLASSIFICATION OF V^2 VOIDS

7.1. Linking Density

While the V^2 algorithm is mostly parameter-free, there is an input parameter in V^2 /VIDE: the maximum zone-linking density, which limits the density of Voronoi cells which can link adjacent zones into voids. The maximum linking density (see Section 5.2 for details) is defined relative to the mean number density of the catalog, \bar{n} , and is equal to $0.2\bar{n}$ by default; it can be as low as 0 (allowing no linking of zones, similar to V^2 /REVOLVER) or it can be left undefined, leading to all zones being linked together into a single void.

While a lower maximum linking density is expected to limit the merging of voids across denser regions, the growth of V^2 voids up to density maxima occurs during the zone creation step, rather than in the subsequent zone-merging step. Consequently, varying the amount of zone merging that occurs is not expected to mitigate the inclusion of the dense shell-crossing region in the void volume of V^2 /VIDE voids.

We examine the effect of the maximum linking density on the distribution of crossing numbers within V^2 /VIDE voids. The central density cut of the V^2 /VIDE algorithm is varied to match the maximum linking density. These results are shown in Table 4. The percent of particles in voids with a given crossing number does not vary by more than $\sim 1\%$ across different linking densities. This is a minor shift compared to the difference between VoidFinder voids and V^2 /VIDE voids ($\sim 12\%$ for both CN= 0 and CN= 3; see Table 1), and still leaves

Table 4. Crossing number distributions

crossing number	maximum linking or central density			
	$0.1\bar{n}$	$0.2\bar{n}$	$0.5\bar{n}$	\bar{n}
0	32.2%	33.0%	33.2%	33.2%
1	20.9%	20.9%	20.8%	20.8%
2	18.5%	18.4%	18.2%	18.2%
3	28.4%	27.7%	27.8%	27.8%

NOTE—Effect of maximum linking or central density on the distribution of crossing numbers within V^2 /VIDE voids. Void-finding was done using a $(111 \text{ Mpc}/h)^3$ subvolume of the Abacus-Summit Hugebase simulation.

the V^2 /VIDE distribution relatively similar to the distribution of all crossing numbers.

7.2. Depth-in-Void

While the centers of V^2 /VIDE voids have similar crossing number distributions to those of VoidFinder voids, this is only out to roughly $0.25R_{\text{eff}}$ (see the middle panel of Figure 3). Restricting the analysis to central regions using distance from the void center is therefore not an effective modification of V^2 , as a significant amount of the void volume is omitted, restricting analysis to a small subset of void regions.

Because V^2 voids generally have irregular shapes, distance from the edge (depth-in-void) may serve as a better measure of centrality than distance from the center, which is more effective for the more spherical voids found by VoidFinder. Zaidouni et al. (2024) show that void galaxies with a normalized distance from the V^2 /VIDE void edge of at least $0.4d_{\text{max}}$ have a distribution of astrophysical properties similar to those of galaxies within VoidFinder voids.

We examine the distribution of crossing numbers at different depths within V^2 voids to determine whether depth is a better measure of centrality than distance from the center. The distance from the void edge is defined as the distance to the nearest polygon making up the surface of the void. The results are shown in Figure 5 for both V^2 and VoidFinder. The previously observed trend of lower crossing numbers for more centrally located void particles is apparent, but just as in the distribution based on distance from the void center (Figure 3), the V^2 voids do not exhibit the sharp wall feature observed in VoidFinder voids. Further, the central regions of voids defined using depths ($1 - d/d_{\text{max}} < 0.25$) do not favor low crossing numbers as strongly as central regions defined using distance from void centers ($r/R_{\text{eff}} < 0.25$).

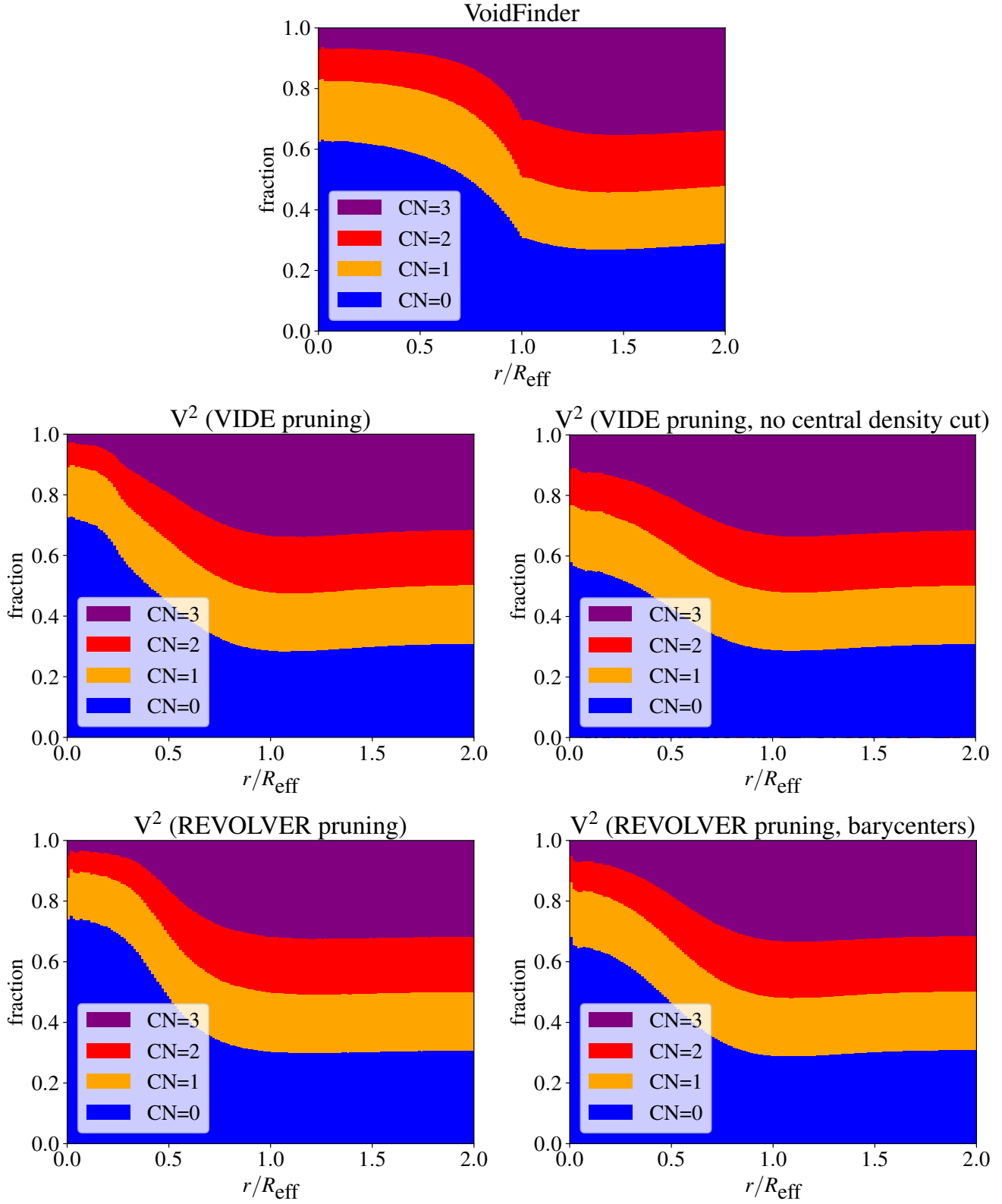


Figure 4. The distributions of crossing numbers by normalized distance from void centers found in redshift space by VoidFinder (top), V²/VIDE (middle), and V²/REVOLVER (bottom).

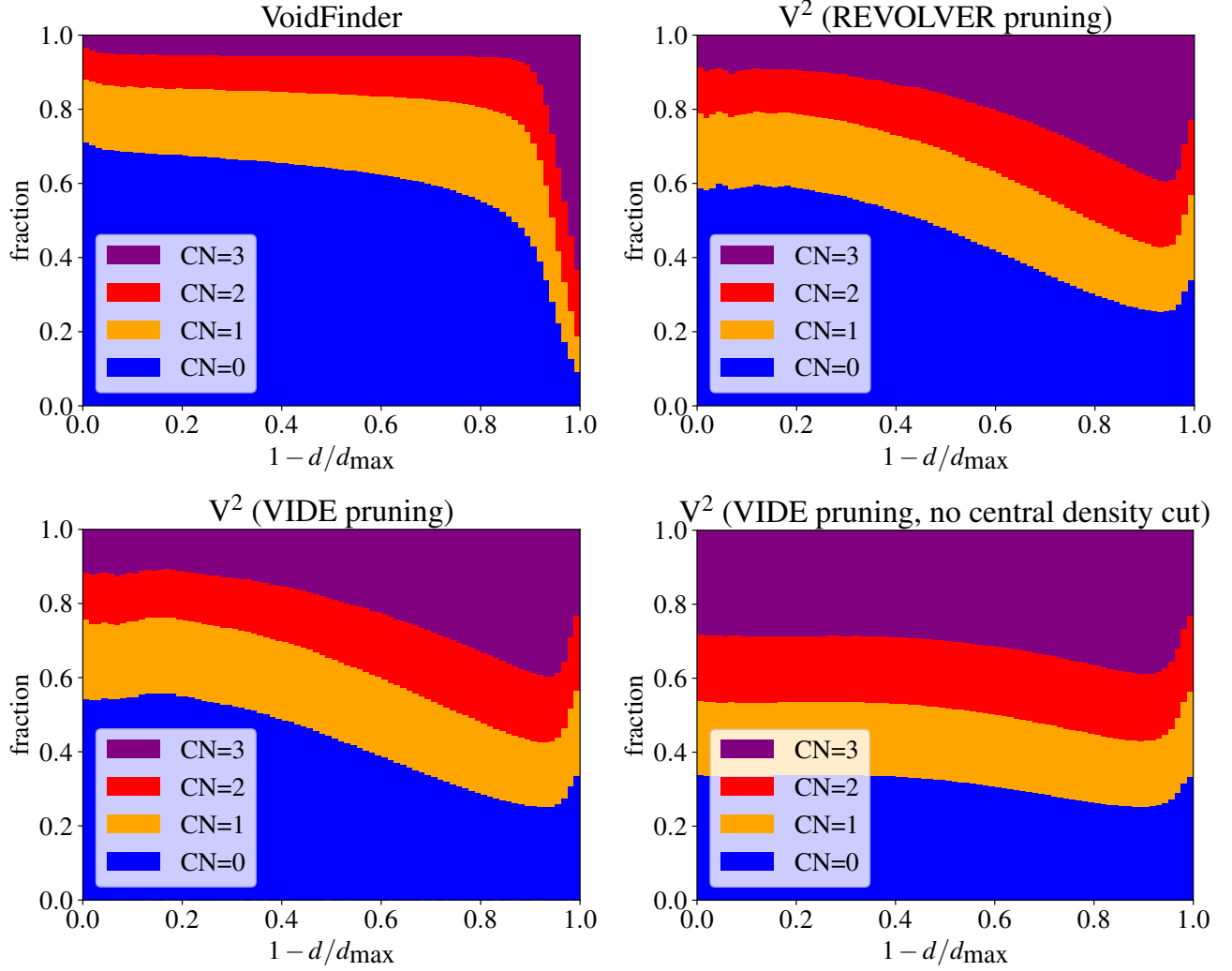


Figure 5. Distribution of crossing numbers by normalized depth from void edges within VoidFinder (top left), V^2 /REVOLVER (top right), and V^2 /VIDE (bottom) voids. Depths were computed only for a $(1 \text{ Gpc}/h)^3$ subvolume of the AbacusSummit Hugebase simulation.

The preference for low crossing numbers is present but particularly weak in the case of V^2 /VIDE with no central density cut. These results indicate that there is no clear method for extracting the dynamically-distinct parts of the void regions from V^2 voids. The shift back to lower crossing numbers at the edge of V^2 voids can be attributed to the fact that these void edges are made up of boundaries between halos' Voronoi cells, an inherently low-density region.

8. CONCLUSIONS

We study the relative accuracy of two different void-finding algorithms in detecting dynamical void regions by examining the positions of their voids relative to non-clustering regions in the dark matter distribution. Using a $(2 \text{ Gpc}/h)^3$ N -body simulation from the AbacusSummit simulation suite (Maksimova et al. 2021), the evolutionary history of each dark matter particle is identified using a modified version of the ORIGAMI algorithm (Falck et al. 2012), which counts the number of dimensions along which dark matter particles have undergone shell-crossing. Identifying particles with crossing number 0 as belonging to voids, we compare their positions with voids found in the corresponding halo distribution by VoidFinder and V^2 , two void-finding algorithms implemented in VAST (Douglass et al. 2022).

We find that while both void-finding algorithms produce voids with a central bias towards lower crossing numbers, this bias gradually diminishes at greater distances from V^2 void centers, while the preference remains strong up to the edge of VoidFinder voids. This suggests that V^2 includes the shell-crossing region surrounding voids as part of the void volume. Further, at the void edge defined as $r/R_{\text{eff}} \approx 1$, voids found by VoidFinder have a preference for higher crossing numbers that is even stronger than the background distribution at larger radii, in good agreement with the shell-crossing predictions of the excursion-set formalism by Sheth & van de Weygaert (2004). This feature is absent in the distribution of crossing numbers around voids found by V^2 .

Given the relative inability of V^2 to identify dynamically-distinct void regions, we attempt several methods to improve the classification of void regions by V^2 . The V^2 /VIDE algorithm has one user-set parameter, the maximum linking density. We find that varying the maximum linking density has little effect on the distribution of crossing numbers within voids. We also examine the crossing number distribution as a function of distance from the void edge (depth) rather than distance from the void center. While void depth has been used to provide a definition of a central region with a stronger preference for void-like galaxy properties (Zaidouni et al. 2024), this did not improve the crossing number profiles of V^2 /VIDE voids. We conclude that VoidFinder more effectively identifies the dynamically-distinct regions primarily occupied by dark matter particles with low crossing number.

The AbacusSummit Hugebase simulation analyzed in this work is one of the largest to be used in a crossing number analysis. We modified the ORIGAMI algorithm (available for downloads at <https://github.com/dveyrat/origami/tree/subdivide>) to allow it to be run on this 2304^3 particle set. These modifications enable similar analyses using other AbacusSummit simulations, such as studies of the effects of different void-finding algorithms on cosmological constraints.

ACKNOWLEDGEMENTS

The authors would like to thank Stephen W. O'Neill, Jr. for his help improving the VoidFinder algorithm in VAST, and Michael Vogeley and Fiona Hoyle for the original VoidFinder code and void-finding expertise. D.V. and S.B. acknowledge support from the U.S. Department of Energy Office of High Energy Physics under the grant DE-SC0008475. K.D. and D.V. acknowledge support from grant 62177 from the John Templeton Foundation.

This research used resources of the National Energy Research Scientific Computing Center (NERSC), a U.S. Department of Energy Office of Science User Facility located at Lawrence Berkeley National Laboratory.

REFERENCES

- Bond, J. R., Cole, S., Efstathiou, G., & Kaiser, N. 1991, *ApJ*, 379, 440, doi: [10.1086/170520](https://doi.org/10.1086/170520)
- Bond, J. R., Kofman, L., & Pogosyan, D. 1996, *Nature*, 380, 603, doi: [10.1038/380603a0](https://doi.org/10.1038/380603a0)
- Chantavat, T., Sawangwit, U., & Wandelt, B. D. 2017, *ApJ*, 836, 156, doi: [10.3847/1538-4357/836/2/156](https://doi.org/10.3847/1538-4357/836/2/156)
- de Lapparent, V., Geller, M. J., & Huchra, J. P. 1986, *ApJL*, 302, L1, doi: [10.1086/184625](https://doi.org/10.1086/184625)
- Douglass, K. A., Smith, J. A., & Demina, R. 2019, *ApJ*, 886, 153, doi: [10.3847/1538-4357/ab4bce](https://doi.org/10.3847/1538-4357/ab4bce)
- Douglass, K. A., Veyrat, D., O'Neill, S. W., et al. 2022, *Journal of Open Source Software*, 7, 4033, doi: [10.21105/joss.04033](https://doi.org/10.21105/joss.04033)
- El-Ad, H., & Piran, T. 1997, *ApJ*, 491, 421, doi: [10.1086/304973](https://doi.org/10.1086/304973)

- Falck, B., & Neyrinck, M. C. 2015, *MNRAS*, 450, 3239, doi: [10.1093/mnras/stv879](https://doi.org/10.1093/mnras/stv879)
- Falck, B. L., Neyrinck, M. C., & Szalay, A. S. 2012, *ApJ*, 754, 126, doi: [10.1088/0004-637X/754/2/126](https://doi.org/10.1088/0004-637X/754/2/126)
- Garrison, L. H., Eisenstein, D. J., Ferrer, D., Maksimova, N. A., & Pinto, P. A. 2021, *Monthly Notices of the Royal Astronomical Society*, 508, 575, doi: [10.1093/mnras/stab2482](https://doi.org/10.1093/mnras/stab2482)
- Geller, M. J., & Huchra, J. P. 1989, *Science*, 246, 897, doi: [10.1126/science.246.4932.897](https://doi.org/10.1126/science.246.4932.897)
- Goldberg, D. M., & Vogeley, M. S. 2004, *ApJ*, 605, 1, doi: [10.1086/382143](https://doi.org/10.1086/382143)
- Gregory, S. A., & Thompson, L. A. 1978, *ApJ*, 222, 784, doi: [10.1086/156198](https://doi.org/10.1086/156198)
- Habouzit, M., Pisani, A., Goulding, A., et al. 2020, *Monthly Notices of the Royal Astronomical Society*, 493, 899, doi: [10.1093/mnras/staa219](https://doi.org/10.1093/mnras/staa219)
- Hadzihiyska, B., Eisenstein, D., Bose, S., Garrison, L. H., & Maksimova, N. 2021, *Monthly Notices of the Royal Astronomical Society*, 509, 501, doi: [10.1093/mnras/stab2980](https://doi.org/10.1093/mnras/stab2980)
- Hamaus, N., Pisani, A., Sutter, P. M., et al. 2016, *PhRvL*, 117, 091302, doi: [10.1103/PhysRevLett.117.091302](https://doi.org/10.1103/PhysRevLett.117.091302)
- Hamaus, N., Wandelt, B. D., Sutter, P. M., Lavaux, G., & Warren, M. S. 2014, *PhRvL*, 112, 041304, doi: [10.1103/PhysRevLett.112.041304](https://doi.org/10.1103/PhysRevLett.112.041304)
- Hoyle, F., Rojas, R. R., Vogeley, M. S., & Brinkmann, J. 2005, *The Astrophysical Journal*, 620, 618, doi: [10.1086/427176](https://doi.org/10.1086/427176)
- Hoyle, F., & Vogeley, M. S. 2002, *ApJ*, 566, 641, doi: [10.1086/338340](https://doi.org/10.1086/338340)
- Jöeveer, M., Einasto, J., & Tago, E. 1978, *MNRAS*, 185, 357, doi: [10.1093/mnras/185.2.357](https://doi.org/10.1093/mnras/185.2.357)
- Kirshner, R. P., Oemler, A., J., Schechter, P. L., & Shectman, S. A. 1981, *ApJL*, 248, L57, doi: [10.1086/183623](https://doi.org/10.1086/183623)
- Lavaux, G., & Wandelt, B. D. 2012, *ApJ*, 754, 109, doi: [10.1088/0004-637X/754/2/109](https://doi.org/10.1088/0004-637X/754/2/109)
- Maksimova, N. A., Garrison, L. H., Eisenstein, D. J., et al. 2021, *Monthly Notices of the Royal Astronomical Society*, 508, 4017, doi: [10.1093/mnras/stab2484](https://doi.org/10.1093/mnras/stab2484)
- Mao, Q., Berlind, A. A., Scherrer, R. J., et al. 2017, *ApJ*, 835, 160, doi: [10.3847/1538-4357/835/2/160](https://doi.org/10.3847/1538-4357/835/2/160)
- Melchior, P., Sutter, P. M., Sheldon, E. S., Krause, E., & Wandelt, B. D. 2014, *MNRAS*, 440, 2922, doi: [10.1093/mnras/stu456](https://doi.org/10.1093/mnras/stu456)
- Nadathur, S., Carter, P. M., Percival, W. J., Winther, H. A., & Bautista, J. E. 2019, *PhRvD*, 100, 023504, doi: [10.1103/PhysRevD.100.023504](https://doi.org/10.1103/PhysRevD.100.023504)
- Neyrinck, M. C. 2008, *MNRAS*, 386, 2101, doi: [10.1111/j.1365-2966.2008.13180.x](https://doi.org/10.1111/j.1365-2966.2008.13180.x)
- Patiri, S. G., Prada, F., Holtzman, J., Klypin, A., & Betancort-Rijo, J. 2006, *Monthly Notices of the Royal Astronomical Society*, 372, 1710, doi: [10.1111/j.1365-2966.2006.10975.x](https://doi.org/10.1111/j.1365-2966.2006.10975.x)
- Pisani, A., Sutter, P. M., Hamaus, N., et al. 2015, *PhRvD*, 92, 083531, doi: [10.1103/PhysRevD.92.083531](https://doi.org/10.1103/PhysRevD.92.083531)
- Planck Collaboration, Aghanim, N., Akrami, Y., et al. 2020, *A&A*, 641, A6, doi: [10.1051/0004-6361/201833910](https://doi.org/10.1051/0004-6361/201833910)
- Press, W. H., & Schechter, P. 1974, *ApJ*, 187, 425, doi: [10.1086/152650](https://doi.org/10.1086/152650)
- Ricciardelli, E., Quilis, V., & Varela, J. 2014, *MNRAS*, 440, 601, doi: [10.1093/mnras/stu307](https://doi.org/10.1093/mnras/stu307)
- Rojas, R. R., Vogeley, M. S., Hoyle, F., & Brinkmann, J. 2005, *ApJ*, 624, 571, doi: [10.1086/428476](https://doi.org/10.1086/428476)
- Sheth, R. K., & van de Weygaert, R. 2004, *Monthly Notices of the Royal Astronomical Society*, 350, 517, doi: [10.1111/j.1365-2966.2004.07661.x](https://doi.org/10.1111/j.1365-2966.2004.07661.x)
- Sutter, P. M., Lavaux, G., Wandelt, B. D., & Weinberg, D. H. 2012, *ApJ*, 761, 187, doi: [10.1088/0004-637X/761/2/187](https://doi.org/10.1088/0004-637X/761/2/187)
- Sutter, P. M., Pisani, A., Wandelt, B. D., & Weinberg, D. H. 2014, *MNRAS*, 443, 2983, doi: [10.1093/mnras/stu1392](https://doi.org/10.1093/mnras/stu1392)
- Sutter, P. M., Lavaux, G., Hamaus, N., et al. 2015, *Astronomy and Computing*, 9, 1, doi: [10.1016/j.ascom.2014.10.002](https://doi.org/10.1016/j.ascom.2014.10.002)
- van de Weygaert, R., & Platen, E. 2011, in *International Journal of Modern Physics Conference Series*, Vol. 1, International Journal of Modern Physics Conference Series, 41–66, doi: [10.1142/S2010194511000092](https://doi.org/10.1142/S2010194511000092)
- Verza, G., Pisani, A., Carbone, C., Hamaus, N., & Guzzo, L. 2019, *JCAP*, 2019, 040, doi: [10.1088/1475-7516/2019/12/040](https://doi.org/10.1088/1475-7516/2019/12/040)
- Zaidouni, F., Veyrat, D., Douglass, K. A., & BenZvi, S. 2024, *arXiv e-prints*, arXiv:2403.20008, doi: [10.48550/arXiv.2403.20008](https://doi.org/10.48550/arXiv.2403.20008)
- Zeldovich, Y. B. 1970, *Astron. Astrophys.* 5: 84-9(Mar 1970). <https://www.osti.gov/biblio/4158113>
- Zhao, C., Chuang, C.-H., Kitaura, F.-S., et al. 2020, *MNRAS*, 491, 4554, doi: [10.1093/mnras/stz3339](https://doi.org/10.1093/mnras/stz3339)
- Zhao, C., Variu, A., He, M., et al. 2022, *MNRAS*, 511, 5492, doi: [10.1093/mnras/stac390](https://doi.org/10.1093/mnras/stac390)